Available online at www.sciencedirect.com

SciVerse ScienceDirect

Ceramics International 39 (2013) 3597–3601

CERAMICS INTERNATIONAL

www.elsevier.com/locate/ceramint

# Synthesis of $Mg_{0.48}Cu_{0.12}Zn_{0.40}Fe_2O_4$ ferrite and its aptness for multilayer chip component application

S.S. Kamble[a,*], Vrushali S. Jagtap[a], P.C. Pingale[b]

[a]*Bharat-Ratna Indira Gandhi College of Engineering, Kegaon, Solapur 413255, M.S., India*
[b]*Tuljaram Chaturchand College, Baramati 413102, M.S., India*

Received 19 August 2012; received in revised form 9 October 2012; accepted 10 October 2012
Available online 17 October 2012

**Abstract**

Here we reported the synthesis of Mg–Cu–Zn ferrite ($Mg_{0.48}Cu_{0.12}Zn_{0.40}Fe_2O_4$) by ceramic and self-sustaining auto-combustion (sucrose) methods. Required oxides in powder form were processed (hand mill = 3 h, pre-sinter = 600 °C for 180 min and final sinter = 910 °C for 9 h) to obtain the ferrite sample through the ceramic methods. Whereas, aqueous metal nitrates along with the sucrose as fuel were processed (at 200 °C, final sinter = 600 °C for 180 min) to obtain ferrite product via the auto-combustion route. As-synthesized ferrite samples were then subjected to crystallographic, structural and magnetic investigations by techniques viz. X-ray diffraction, IR spectroscopy and B–H measurements. Purity and phase formation were confirmed by XRD examinations. Cation redistribution was also suggested by XRD analyses which supplement the variation of magnetic properties. IR absorption bands were found to be in the expected high frequency range (574.95 $cm^{-1}$ and 582.39 $cm^{-1}$) and low frequency range ($\approx$ 431 $cm^{-1}$) which fortifies the spinel phase formation. Boost in magnetic performance of sucrose methods' yield was observed owing to reduced porosity and increased surface area. Thus, Mg–Cu–Zn ferrite prepared via the self-sustaining auto-combustion route has superior magnetic properties at relatively low sintering temperature and can be employed in multi-layer chip application readily.


*Keywords:* Ferrite; Ceramic; Chemical synthesis; IR spectroscopy

## 1. Introduction

Multi-layer ferrite chip components are fabricated by laminating sheets of ferrite and silver as metallization for the internal coil windings. Melting point of silver is 961 °C, hence restricting the co-firing temperature below 950 °C. Ferrites for multilayer components, therefore, have to exhibit a good sintering activity to form dense layers with optimized properties at $T < 950$ °C.

NiCuZn ferrites were developed as the standard ferrite materials for the fabrication of multilayer chip components [1]. However, they still have unresolved issues like stresses of internal windings, compatibility with silver and its mobility in the ferrite. Moreover, nickel oxide raw materials are hazardous and of high cost, hence it would be advantageous to replace Ni with another metal in the ferrite material.

Mg–Cu–Zn ferrite can be prepared by various methods like hydrothermal, co-precipitation, combustion, sol–gel, precursor etc. The Auto-combustion route follows highly exothermic redox reaction between metal nitrates and fuel to produce the final product. Prime advantage of auto-combustion process is the nano-scale yield with the use of inexpensive equipments. Additionally, the technique is ideally suited for the products with the improved sintering activity owing to the enhanced surface area.

Major advantages of the auto-combustion method are as follows:

- Highly reactive product due to nano-size.
- Involvement of low processing temperature.
- Metal nitrates and an organic fuel are mixed in water to form an aqueous solution, hence, molecular mixing of the components.

*Corresponding author. Tel.: +91 9970 836665.
*E-mail address:* shrishail_kamble@yahoo.co.in (S.S. Kamble).

0272-8842/$ - see front matter © 2012 Elsevier Ltd and Techna Group S.r.l. All rights reserved.
http://dx.doi.org/10.1016/j.ceramint.2012.10.187

- Instead of using a high temperature furnace to supply the energy needed for the component oxides to react , the auto-combustion reaction itself supplies the energy.

In the present communication Mg–Cu–Zn ferrite was prepared by the ceramic as well as self-sustaining auto-combustion route (sucrose method). The sucrose method wasas born from a process called proteic sol–gel in which the coconut water (protein present in coconut water) acts as a chelating agent for the development of oxides [2]. In order to reduce production cost further, sucrose was used as an alternative for coconut water [3].

## 2. Materials and methods

$Mg_{0.48}Cu_{0.12}Zn_{0.40}Fe_2O_4$ ferrite was prepared by ceramic and self-sustaining auto-combustion processes. For the ceramic route stoichiometric amounts of desired analytical reagent (AR) grade oxide powders (MgO, CuO, ZnO and $Fe_2O_3$) in required proportion were hand milled for 3 h in acetone media and pre-sintered at 600 °C for 180 min. This pre-sintered powder was then again hand milled for 2 h and uniaxially pressed at a pressure of 7 t/in.$^2$ to form pellets. These pellets were then finally sintered at 910 °C for 9 h.

In case of the self-sustaining auto-combustion (sucrose) method stoichiometric amounts of desired AR grade metal nitrates were dissolved in distilled water by maintaining ratio of metal ion concentration to $Fe^+$ ion concentration as 1:2 (0.712 mol $Mg(NO_3)_2 \cdot 6H_2O$, 0.178 mol $Cu(NO_3)_2 \cdot 3H_2O$, 0.593 mol $Zn(NO_3)_2 \cdot 6H_2O$ and 2.966 mol $Fe(NO_3)_3 \cdot 9H_2O$). Aqueous solution of metal nitrates, 0.8 mol of 10% (W/V) aqueous polyvinyl alcohol (PVA) and the aqueous solution of sucrose (4 mol metal ion) were mixed together to form metal nitrate–sucrose–PVA solution, which was then evaporated to a viscous liquid (at 80 °C). Complete evaporation of viscous liquid (at 200 °C) results in the formation of carbonaceous black colored fluffy mass that was then ground to fine powder. The ground powder was then uniaxially pressed at the pressure of 7 t/in.$^2$ to form pellets. Pellets thus formed were finally sintered at 600 °C for 180 min.

As-synthesized ferrite products were characterized by using powder X-ray diffraction and Infrared spectra (IR) techniques. Philips PW-3710 X-ray diffractometer (Cu$K\alpha$=1.5424 Å) was used for XRD analysis. IR spectra of finely crushed ferrite samples were recorded using a Perkin-Elmer 783 spectrophotometer from 300 to 800 cm$^{-1}$ by the KBr pellet method. Magnetic properties were measured at room temperature using a high-field hysteresis loop tracer in the applied field of 1.6 kOe and 2 kOe. From the obtained $B$–$H$ plots, the saturation magnetization ($M_s$), remanence magnetization ($M_r$) and coercivity ($H_c$) were determined.

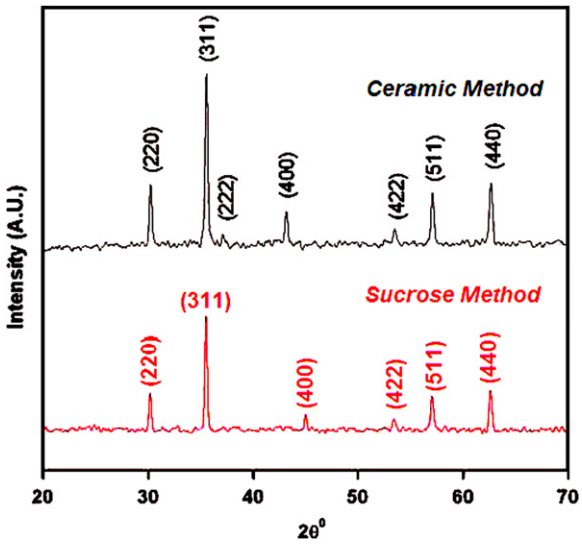


Fig. 1. X-ray diffractograms for Mg–Cu–Zn ferrite.

## 3. Results and discussion

### 3.1. XRD analysis

As-obtained ferrite samples were characterized for structural analysis by using the X-ray diffraction technique. From X-ray diffractograms (Fig. 1), formation of cubic spinel phase is perceived and all XRD peaks are in consonance with the JCPDS card no. 08–0234 and earlier reports [4]. Variation in XRD peak intensities for ceramic and sucrose methods was also observed from the diffractograms. According to the X-ray diffraction principle, change in XRD peak intensity is generally caused by the change of structure factor which further depends on atom kind, quantity and position of atom in the cell. Besides, grain size, micro-strain, non-uniform lattice distortions, grain surface relaxation, solid solution inhomogeneity and temperature factors are also responsible for such variation in peak intensity.

The average grain size and lattice constant were determined by fitting the most intense diffraction peak (311) to Gaussian function and using the Debye–Scherrer formula. The X-ray density of ferrite samples was estimated by using the relation

$$X\text{-ray density } (\rho_{\text{ferrite}}) = \sum \frac{8M}{Na^3}$$

where $M$ is the molecular weight of particular ferrite, $N$ is the Avogadro number and $a$ is the lattice constant.

The actual density $\rho_a$ of ferrite samples was also measured by employing the Archimedes principle. By having the knowledge of actual density and X-ray density, the percentage of porosity (%$P$) in each sample was calculated.

Shift in peak positions and the difference in lattice parameter can be credited to the change in $Mg^{2+}$ ion distribution on A-sites, taking into account the fact that copper ions prefer the B-sites [5]. $Zn^{2+}$ ions on the A-sites exhibit a smaller ionic radius than on the B-sites because of

Table 1
Table of XRD analysis for $Mg_{0.48}Cu_{0.12}Zn_{0.40}Fe_2O_4$ ferrite.

| Ceramic method | | | Sucrose method | | |
|---|---|---|---|---|---|
| $2\theta^{\circ}$ | (*hkl*) | $d_{hkl}$ (Å) | $2\theta^{\circ}$ | (*hkl*) | $d_{hkl}$ (Å) |
| 30.30 | (220) | 2.9639 | 30.11 | (200) | 2.9636 |
| 35.77 | (311) | 2.5287 | 35.45 | (311) | 2.5273 |
| 37.21 | (222) | 2.3842 | 45.03 | (400) | 2.0956 |
| 43.28 | (400) | 2.0957 | 53.39 | (422) | 1.7110 |
| 53.77 | (422) | 1.7126 | 56.93 | (511) | 1.6131 |
| 57.14 | (511) | 1.6167 | 62.51 | (440) | 1.4818 |
| 62.78 | (440) | 1.4854 | – | – | – |

Table 2
Data on lattice parameter (***a***), particle size ($D^{-}$), X-ray density ($\rho_x \times 10^3$ **kg/m$^3$**), actual density ($\rho_a \times 10^3$ **kg/m$^3$**), and porosity (% ***P***) for $Mg_{0.48}Cu_{0.12}Zn_{0.40}Fe_2O_4$ ferrite.

| Preparation method | *a* (Å) | $D^{-}$(μm) | $\rho_x$ | $\rho_a$ | % *P* |
|---|---|---|---|---|---|
| Ceramic | 8.38 | 0.27 | 4.97 | 5.25 | 5.33 |
| Sucrose | 8.36 | 34.16 | 5.02 | 5.09 | 1.37 |

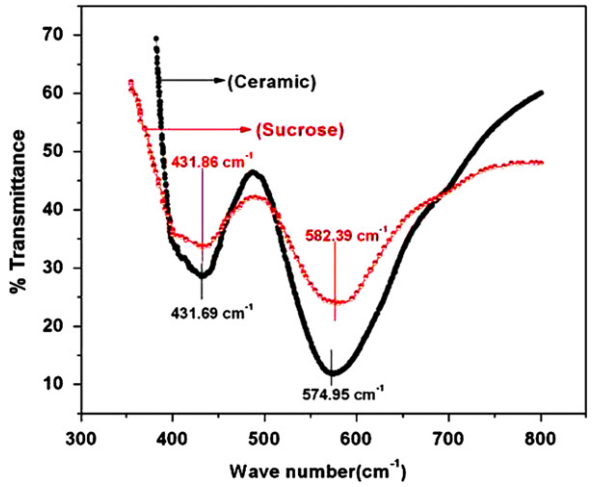


Fig. 2. IR absorption spectra of Mg–Cu–Zn ferrite.

covalence effects [6]. Thus the remarkable shift in peak positions is due to the redistribution of the $Mg^{2+}$ ions.

Data on XRD analysis is provided in Tables 1 and 2.

### 3.2. Infrared absorption spectroscopy

IR absorption spectrum is an essential tool used for study of the ionic positions though vibrational mode analysis [7,8]. According to Waldron's classification [9], the vibrations of the unit cell of cubic spinel can be construed in the tetrahedral (A-site) and octahedral (B-site) sites. So, the absorption band $\upsilon_1$ is caused by the stretching vibration of the tetrahedral metal–oxygen bond, and the absorption band $\upsilon_2$ is caused by the metal–oxygen vibrations in octahedral sites.

The IR absorption spectra (Fig. 2) of finely crushed ferrite samples were obtained by using KBr as solvent in the wave number range of 300 $cm^{-1}$–800 $cm^{-1}$. Cation–oxygen bond (A–O) lengths for the octahedral and tetrahedral sites were calculated by using the formulae [10]

$$(\text{Tetrahedral bond length})—d_{AX} = \sqrt{3}(u-1/4)a$$

$$(\text{Octahedral } b\text{ond } l\text{ength})—d_{BX} = \left(3u^2 - \frac{11u}{4} + \frac{43}{64}\right)^{1/2} a$$

where $a$ is the lattice parameter and $u$ is the oxygen diffusion parameter.

The absorption bands for Mg–Cu–Zn ferrite samples were found to be in the expected frequency range fortifying the cubic spinel phase formation [11].

The difference in the frequencies between $\upsilon_1$ and $\upsilon_2$ is due to changes in bond length ($Fe^{3+}$–$O^{2-}$) at octahedral and tetrahedral sites [8]. In the present spectra for sample prepared via the ceramic route, $\upsilon_1$ band appears at 574.95 $cm^{-1}$ and it increases to 582.39 $cm^{-1}$ for auto-combustion yield. Similarly, the second absorption band $\upsilon_2$ for ceramic sample appears at 431.69 $cm^{-1}$ and it is also found to increase slightly to 431.86 $cm^{-1}$ for sucrose sample. The change in the band position is expected because of the difference in the $Fe^{3+}$–$O^{2-}$ distances for the octahedral and tetrahedral complexes. Thus, these shifts in the band frequencies could be explained on the basis of the change in the bond length due to cation redistribution that causes variations in the cation–oxygen bond (A–O) length for the octahedral and tetrahedral groups [12,13].

The values of the force constants $f_T$ and $f_O$ for the tetrahedral and the octahedral sites (Table 3) were calculated by using the relation [14].

$$f = 4\pi^2 c^2 v^2 \mu$$

where $c$ is the speed of light $2.99 \times 10^8$ m/s, $v$ is the vibration frequency of tetrahedral and the octahedral sites, and $\mu$ is the reduced mass for $Fe^{3+}$ ions and the $O^{2-}$ ions.

### 3.3. Magnetic properties

Cation distribution, particle size and density of the product are the factors that influence the magnetic properties of ferrite. The magnetic properties of the as-prepared ferrite samples were analyzed by the magnetic hysteresis loop at room temperature. High-field hysteresis loop tracer was used for the investigations of magnetization ($B$–$H$) curves. Magnetization curves revealed an increase in coercive field ($H_c$), remanent magnetization ($M_r$) and saturation magnetization ($\sigma_s$) for sucrose methods' yield. At the applied magnetic field of 1.6 kOe (Fig. 3) saturation magnetization was found to be 43.27 emu/g and 53.39 emu/gm for the ceramic and sucrose method sample respectively. And, at the applied magnetic field of 2 kOe

Table 3
Tetrahedral band ($\upsilon_1$), octahedral band ($\upsilon_2$), bond lengths, tetrahedral force constant ($f_T$) and octahedral force constant ($f_O$) for $Mg_{0.48}Cu_{0.12}Zn_{0.40}Fe_2O_4$ ferrite.

| Preparation method | $\upsilon_1$ ($cm^{-1}$) | $\upsilon_2$ ($cm^{-1}$) | Bond length (Å) | | $f_T$ | $f_O$ |
|---|---|---|---|---|---|---|
| | | | Tetrahedral | Octahedral | dyn/cm | dyn/cm |
| Ceramic | 574.95 | 431.69 | 1.9740 | 2.0042 | 240.45 | 135.55 |
| Sucrose | 582.39 | 431.86 | 1.9749 | 2.0051 | 246.72 | 135.66 |

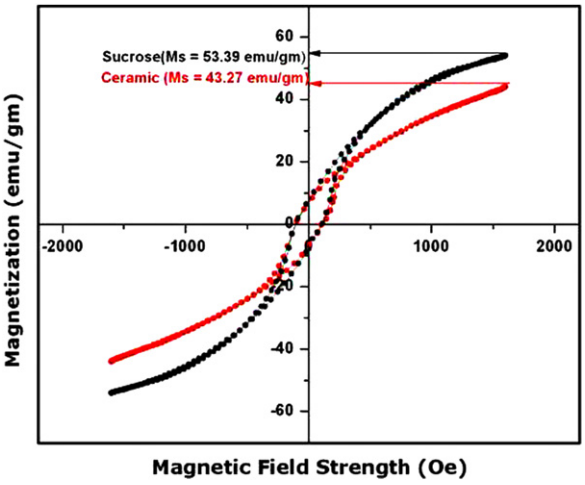


Fig. 3. *B–H* measurement at 1.6 kOe magnetic field.

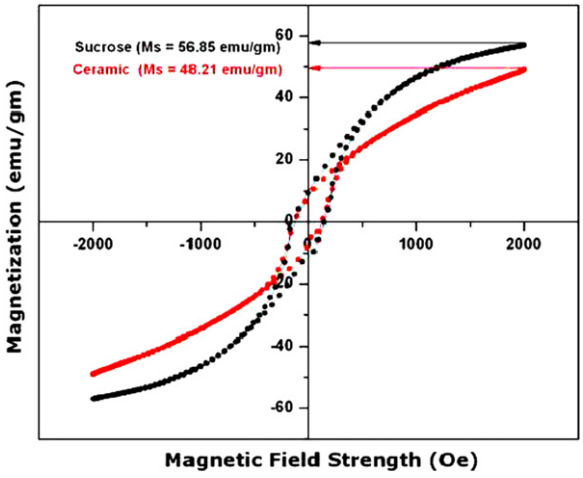


Fig. 4. *B–H* measurement at 2 kOe magnetic field.

(Fig. 4) saturation magnetization was found to be 48.21 emu/g and 56.85 emu/gm for the ceramic and sucrose method sample respectively.

Unquestionably, the ferrite prepared by the sucrose method has better-quality magnetic properties depending upon the redistribution of cations on A and B sites of spinel ferrite. In other words, the superior magnetic behavior of sucrose sample could be attributed to the migration of little $Fe^{3+}$ ions from B site to A site via conversion of a number of $Fe^{2+}$ ions to $Fe^{3+}$ ions with subsequent increase in the $Fe_A^{3+}$–$Fe_B^{3+}$ super-exchange interactions which give rise to spin canting and surface spin disorder [15]. In addition, conversion of $Fe^{2+}$ ions to $Fe^{3+}$ brought about a reduction in crystalline size of ferrite prepared by sucrose method which can be correlated to the difference of ionic radii in both ferric and ferrous ions.

The individual grain acts as a magnetic material having a certain amount of saturation magnetization. These grains together form a magnetic circuit to produce resultant saturation magnetization. The presence of pores breaks the magnetic circuits present among the grains and results in a net reduction of magnetic properties with decreasing density [16], hence decreased porosity of sucrose yield is one of the reasons for enhanced magnetic property. Particle size also affects the magnetic properties as the domain size depends on it. If the particle size is quite large and consists of several domains, the magnetization in the direction of applied magnetic field takes place by domain wall displacement as well as by domain magnetization rotation. If the volume of the particle is reduced in such a way that it contains only single domain, then its change in magnetization takes place by rotation only, as a result of which the coercivity increases [17,18]. The formation and width of domain walls in multi-domain grains depend on crystal anisotropy energy. Hence the domain wall width and domain wall thickness were also calculated (Table 4) using the relation [19],

$$D_W = \left(2\frac{k_B T_C}{K_1 a}\right)^{1/2} \times 10^{-2}\ m$$

$$D_t = \left(\frac{k_B T_C}{K_1 a^3}\right)^{1/2} \times 10^{-6}\ m$$

where, $k_B$ is Boltzmann constant, $T_c$ is the curie temperature = 160 °C [20], $K_1$ is the anisotropy constant and $a$ lattice parameter.

An attempt was made to calculate the anisotropy constant ($K$) and the magnetic moment per formula unit in the Bohr magneton ($n_B$) by using the following relations [21]:

$$n_B = \frac{M\sigma_S}{5585}$$

$$H_C = \frac{MK_1}{\sigma_S}$$

Table 4
Values for coercive field ($H_c$), saturation magnetization ($\sigma_S$), remanent magnetization ($M_r$), anisotropy constant ($K$), domain wall width ($D_W$) and domain wall thickness ($D_T$) of Mg–Cu–Zn ferrite.

| At 1.6 kOe | | | | | | |
|---|---|---|---|---|---|---|
| **Preparation method** | $H_c$ **(Oe)** | $\sigma_S$ **(emu/gm)** | $M_r$ **(emu/gm)** | $-K_1$ **( $\times 10^2$ J/m3)** | $D_W$ **(μm)** | $D_T$ **(μm)** |
| Ceramic | 97.40 | 43.27 | 6.62 | 3.9 | 1.164 | 0.981 |
| Sucrose | 99.03 | 53.39 | 7.48 | 4.8 | 1.041 | 0.887 |
| | | | **At 2 kOe** | | | |
| **Preparation method** | $H_c$ **(Oe)** | $\sigma_S$ **(emu/gm)** | $M_r$ **(emu/gm)** | $-K_1$ **( $\times 10^2$ J/m$^3$)** | $D_W$ **(μm)** | $D_T$ **(μm)** |
| Ceramic | 120.13 | 48.21 | 7.71 | 5.3 | 0.998 | 0.841 |
| Sucrose | 146.10 | 56.85 | 9.84 | 7.6 | 0.833 | 0.705 |

where $M$ is the molecular weight of particular composition, $H_c$ is the coercivity, $\sigma_s$ is the saturation magnetization and $K_1$ is the magneto-crystalline anisotropy constant.

## 4. Conclusions

The presented article emphasizes the comparative discussion of Mg–Cu–Zn ferrite prepared via ceramic and self-sustaining auto-combustion (sucrose) methods. Formation and purity of spinel phase were confirmed by XRD and IR absorption spectroscopy. Cations redistribution on the A sites and B sites of spinel phase induced XRD peak shifting. Consequently, spin canting and surface spin disorder persuade magnetic behavior of sucrose methods' yield. Thus, sucrose methods' nanoscale yield has a superior magnetic behavior with the improved sintering activity owing to the enhanced surface area which can facilitate the co-firing of ferrite with silver in multi-layer chip application.

## References


[1] Zhenxing Yue, Ji Zhou, Longtu Li, Hongguo Zhang, Zhilun Gui, Synthesis of nanocrystalline NiCuZn ferrite powders by sol–gel auto-combustion method, Journal of Magnetism and Magnetic Materials 208 (2000) 55–60.

[2] M.A. Macêdo, M.N.B. Silva, A.R. Cestari, E.F.S. Vieira, J.M. Sasaki, J.C. Góes, J. Albino Aguiar, Chitosan-based ferrimagnetic membrane, Physica B: Condensed Matter 354 (2004) 171–173.

[3] E.A. Souza, J.G.S. Duque, L. Kubota, C.T. Meneses, Synthesis and characterization of NiO and $NiFe_2O_4$ nanoparticles obtained by a sucrose-based route, Journal of Physics and Chemistry of Solids 68 (2007) 594–599.

[4] A. Bhaskar, B. Rajini Kanth, S.R. Murthy, Preparation of low-power loss MgCuZn ferrites using the microwave sintering method, Journal of Materials Science 39 (2004) 3787–3791.

[5] A.B. Naik, S.A. Patil, J.I. Powar, X-ray and magnetization studies on Li–Cu mixed ferrites, Journal of Materials Science Letters 7 (1988) 1034–1036.

[6] G. Blasse, Philips Research Reports Supplement 3 (1964) 91.

[7] M. Ishii, M. Nakahira, T. Yamanaka, Infrared absorption spectra and cation distributions in $(Mn, Fe)_3O_4$, Solid State Communications 11 (1972) 209–212.

[8] V.R.K. Murthy, S. Chitra Sonkar, K.V. Reddy, J. Sobhanadri, Indian Journal of Pure and Applied Physics 16 (1978) 79.

[9] R.D. Waldron, Physical Review 99 (1955) 1727–1735.

[10] Tahir Abbas, Y. Khan, Mushtaq Ahmad, Shahid Anwar, X-ray diffraction study of the cation distribution in the Mn–Zn-ferrites, Solid State Communications 82 (1992) 701–703.

[11] Y. Atassi, M. Tally, Low sintering temperature of Mg–Cu–Zn ferrite prepared by the citrate precursor method, Journal of the Iranian Chemical Society 3 (2006) 242–246.

[12] C.B. Kolekar, P.N. Kamble, A.S. Vaingankar, Thermoelectric power in $Gd^{3+}$-substituted Cu–Cd ferrites, Bulletin of Materials Science 18 (1995) 133–140.

[13] G. Chandrasekaran, S. Selvanandan, K. Manivan Nane, Electrical and FTIR studies on Al substituted Mn–Zn mixed ferrites, Journal of Materials Science: Materials in Electronics 15 (2004) 15–18.

[14] S.A. Mazen, H.M. Zaki, S.F. Mansour, Infrared absorption and dielectric properties of Mg–Zn ferrite, International Journal of Pure and Applied Physics 3 (2007) 40–48.

[15] Anjali Verma, Ratnamala Chatterjee, Effect of zinc concentration on the structural, electrical and magnetic properties of mixed Mn–Zn and Ni–Zn ferrites synthesized by the citrate precursor technique, Journal of Magnetism and Magnetic Materials 306 (2006) 313–320.

[16] R.S. Devan, Y.D. Kolekar, B.K. Chougule, Effect of cobalt substitution on the properties of nickel–copper ferrite, Journal of Physics: Condensed Matter 18 (2006) 9809–9821.

[17] K. Mandal, S. Pan Mandal, P. Agudo, M. Pal, A study of nanocrystalline (Mn–Zn) ferrite in $SiO_2$ matrix, Applied Surface Science 182 (2001) 386–389.

[18] Qingqing Fang, Wei Zhong, Zhiqiang Jin, Youwei Du, New modified Sr-ferrite particles for high density magnetic recording, Journal of Applied Physics 85 (1999) 1667–1669.

[19] F.N. Bradley, in: Materials for magnetic functions, Hyden, New York, 1971.

[20] Ji Zhenxing Yue, Longtu Zhou, Xiaohui Li, Wang, Zhilun Gui, Effect of copper on the electromagnetic properties of Mg–Zn–Cu ferrites prepared by sol–gel auto-combustion method, Materials Science and Engineering: B 86 (2001) 64–69.

[21] Sonal Singhal, Kailash Chandra, Cation distribution and magnetic properties in chromium-substituted nickel ferrites prepared using aerosol route, Journal of Solid State Chemistry 180 (2007) 296–300.